Vibration Control for a Cantilever Beam with an Eccentric Tip Mass Using a Piezoelectric Actuator and Sensor

Haigen Yang

Nanjing University of Posts and Telecommunications, Nanjing, China, 210094

(Received 29 August 2015; accepted 26 August 2016)

A novel model using the transfer matrix method for multibody system (TMMMS) is put forward to describe the dynamic characteristics of a cantilever beam that has a concentrated mass at its tip under axial excitations. The theoretical analysis and numerical results demonstrate that this model has some advantages, such as for a small matrix and a higher computational speed. Based on this model a control system, which is composed of a LQG controller, a piezoelectric actuator, and a sensor for the cantilever beam is proposed, theoretically analyzed, and experimentally verified. The experimental results show that the proposed controller with the piezoelectric actuator can effectively reduce the vibration of the cantilever beam with an eccentric tip mass. The piezoelectric sensor can measure vibration responses with high-accuracy. Therefore, this new model gives a broad range of possibilities for model-based controller design and implementation.

1. INTRODUCTION

A cantilever beam with an eccentric tip mass is a familiar dynamic model for mechanical systems. For instance, it may be used to investigate flexible robot arms,[1] mast antenna structures,[1,2] wind tunnel stings carrying an airplane,[3] and Stockbridge dampers used for damping out aeolian vibrations on high-voltage transmission lines.[4] Therefore, it is critical to analyze its vibration characteristics and to design an active vibration controller.[5] The mechanical vibrations of cantilever beams have attracted plenty of attention from researchers over the past several years. The majority of the literature has focused on deriving and solving the exact frequency equation for the particular case of a concentrated mass and/or moment of inertia at the tip.[6]

However, some problems still exist; the first problem of mechanical vibrations on a cantilever beam with a tip mass continues to attract the attention of the research community due to a wide range of practical situations for which such a mechanical system is a reasonable idealization. The second problem is that it is difficult to design a proper vibration controller based on those previous works due to the large size of the matrix of the dynamic equations.[7]

With the developments in sensor/actuator technologies, many researchers have concentrated on vibration control using smart materials such as shape memory alloys (SMAs), and piezoelectric transducers. Piezoelectric materials have been applied in structural vibration control as well as in structural acoustics because of their fast response, large force output, and because they generate no magnetic field in the conversion of electrical energy into mechanical motion.[8–12] Positive position feedback (PPF) was devised by Goh and Caughey[13] and has several distinguished advantages.[14] It has proven to be a solid vibration control strategy for flexible systems with smart materials, particularly with the piezoelectric actuator.[14–17] PPF is essentially a second-order filter that is used to apply high frequency gain stabilization by improving the frequency rolloff of the system.[18] Alternatively, PPF works by using a second-order system which is forced by the position response of the structure. This response is then fed back to give the force input to the structure. To apply PPF, the natural frequencies of the structure should be known. The effectiveness of PPF will deteriorate if the natural frequencies are not well known or have changed for some reason, such as the presence of a tip mass.

As such, in order to reduce the size of matrix of the dynamic equations, we introduce TMMMS to describe the dynamic characteristics of the system and design a LQG control system, which is composed of a LQG controller, a piezoelectric actuator, and a sensor.

TMMMS is a new method of multibody system dynamics (MSD) developed by Rui and his co-workers.[19,20] The highlights of this method are as follows: study MSD without global dynamics equations of the system, keep a low order of the system matrix, and avoid the difficulties in computation caused by high-order matrices. Nowadays, TMMMS has been widely applied to various engineering cases such as for such features without the global dynamics equations of a system, low order of involved system matrix, fast computational speed, and high automation in programming.

2. DYNAMIC MODELING

A sketch of a uniform cantilever beam carrying a rigidly mounted mass is shown in Fig. 1, which is consist of a rigid body (1) and a beam (2). The mass and inertia relative to the centroid of the rigid body are m and J_c, respectively. The beam is an Euler-Bernoulli beam, which has a flexural rigidity, linear density, and length are EI, $\bar{m}$, and L, respectively.

2.1. State Vectors

The state vectors of the connection point among any bodies and hinges vibrating are defined as:

$$\mathbf{z}_{k,j} = [y, \theta_z, m_z, q_y]^{\mathrm{T}}; \tag{1}$$

$$\mathbf{Z}_{k,j} = [Y, \Theta_z, M_z, Q_y]^{\mathrm{T}}; \tag{2}$$

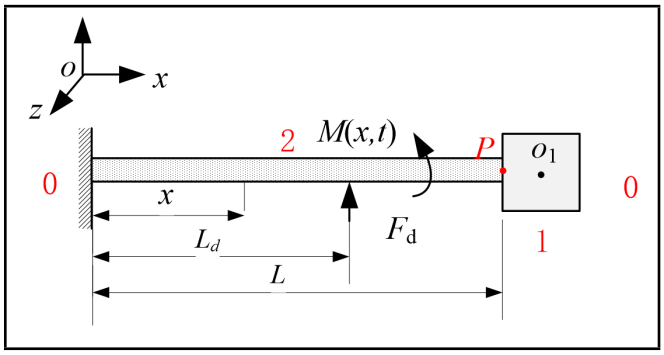

Figure 1. A sketch of the mechanical system being investigated; includes a cantilever beam with an eccentric tip mass.

where Y is the corresponding modal coordinate of the physics coordinate of displacement y relative to the equilibrium position in inertial coordinate system, Θ_z is corresponding modal coordinate of physics coordinate of angular displacement relative to the equilibrium position θ_z, M_z is corresponding modal coordinate of physics coordinate of internal torque m_z of the system, Q_y is corresponding modal coordinate of physical coordinate of internal force q_y the system, and the subscript k is the body indices and j is the hinge indices.

For the natural vibrations of a linear multibody system, the physics coordinates of displacement and interior force can be assumed to be:

$$\mathbf{z}_{k,j} = \mathbf{Z}_{k,j} \mathrm{e}^{\mathrm{i}\omega t}; \tag{3}$$

where ω is the eigenfrequency of the system.

2.2. Transfer Equations and Transfer Matrices

Based on the EulerBernoulli beam theory, the transfer equations of elements can be given by:

$$\mathbf{Z}_{1,0} = \mathbf{U}_1 \mathbf{Z}_{1,2}; \tag{4}$$

$$a\mathbf{Z}_{1,2} = \mathbf{U}_2 \mathbf{Z}_{2,0}. \tag{5}$$

The transfer matrices can be written as:

$$\mathbf{U}_1 = \begin{bmatrix} 1 & a_{\mathrm{O}} & 0 & 0 \\ 0 & 1 & 0 & 0 \\ m\omega^2(a_{\mathrm{O}}-a_{\mathrm{C}}) & -\omega^2[J_{\mathrm{I}}-m(b_{\mathrm{O}}b_{\mathrm{C}}+a_{\mathrm{O}}a_{\mathrm{C}})] & 1 & a_{\mathrm{O}} \\ m\omega^2 & m\omega^2 a_{\mathrm{C}} & 0 & 1 \end{bmatrix}; \tag{6}$$

$$\mathbf{U}_2(x_2) = \begin{bmatrix} S(\lambda x) & \frac{T(\lambda x)}{\lambda} & \frac{U(\lambda x)}{EI\lambda^2} & \frac{V(\lambda x)}{EI\lambda^3} \\ \lambda V(\lambda x) & S(\lambda x) & \frac{T(\lambda x)}{EI\lambda} & \frac{U(\lambda x)}{EI\lambda^2} \\ EI\lambda^2 U(\lambda x) & EI\lambda V(\lambda x) & S(\lambda x) & \frac{T(\lambda x)}{\lambda} \\ EI\lambda^3 T(\lambda x) & EI\lambda^2 U(\lambda x) & \lambda V(\lambda x) & S(\lambda x) \end{bmatrix}; \tag{7}$$

where $(a_{\mathrm{C}}, b_{\mathrm{C}})$ and $(a_{\mathrm{O}}, b_{\mathrm{O}})$ are the coordinates of the centroid of the rigid body and the output point in the connecting body coordinate system, respectively, J_{I} is the inertia of the rigid body relative to the input point, $\lambda = \sqrt[4]{\bar{m}\omega^2/EI}$, $S(x) = (\cosh x + \cos x)/2$, $T(x) = (\sinh x + \sin x)/2$, $U(x) = (\cosh x - \cos x)/2$, and $V(x) = (\sinh x - \sin x)/2$.

Table 1. Parameters of the system.

Rigid body (1)	mass	$m_1 = 7.8$ kg
	inertia	$J_{\mathrm{C}} = 0.013$ kg·m^2
Beam (2)	flexural rigidity	$EI = 244$ N·m^2
	length	$L = 0.5$ m
	linear density	$\bar{m} = 0.94$ kg/m

The overall system transfer equation and overall transfer matrix can be assembled and calculated as:

$$\mathbf{U}_{\mathrm{all}} \mathbf{Z}_{\mathrm{all}} = 0; \tag{8}$$

where $\mathbf{U}_{\mathrm{all}} = \begin{bmatrix} -\mathbf{I}_4 & \mathbf{U}_1\mathbf{U}_2 \end{bmatrix}$, $\mathbf{Z}_{\mathrm{all}} = \begin{bmatrix} \mathbf{Z}_{1,0}^{\mathrm{T}} & \mathbf{Z}_{2,0}^{\mathrm{T}} \end{bmatrix}^{\mathrm{T}}$.

The boundary conditions are:

$$\begin{aligned} \mathbf{Z}_{1,0} &= [Y, \Theta_z, 0, 0]_{1,0}^{\mathrm{T}} \\ \mathbf{Z}_{2,0} &= [0, 0, M_z, Q_y]_{2,0}^{\mathrm{T}}. \end{aligned} \tag{9}$$

When Eq. (9) is substituted into Eq. (8), we get:

$$\bar{\mathbf{U}}_{\mathrm{all}} \bar{\mathbf{Z}}_{\mathrm{all}} = 0; \tag{10}$$

where $\bar{\mathbf{U}}_{\mathrm{all}}$ is a fourth-order square composed of the 1, 2, 7, and 8 columns of $\mathbf{U}_{\mathrm{all}}$, $\bar{\mathbf{Z}}_{\mathrm{all}} = [Y, \Theta_z, M_z, Q_y]^{\mathrm{T}}$. Therefore, the eigenfrequency equation can be expressed as:

$$\det \bar{\mathbf{U}}_{\mathrm{all}} = 0. \tag{11}$$

When the eigenfrequency equation was solved, we got the eigenfrequencies ω_k $(k = 1, 2, 3, \cdots)$. Using the transfer equations given by Eqs. (4) to (8) for each ω_k, the state vector of any point and eigenvectors of the system was obtained easily.

A set of numerical simulations with the parameters listed in Tab. 2.2 were carried out to assess the effects of some methods on calculating the natural frequencies of the system. Table 2.2 lists the first six natural frequencies versus different methods, which indicates that the computational results obtained by the TMMMS and the Newton-Euler method[21] are in agreement and the TMMMS can improve the computational accuracy than the finite element method.

2.3. Dynamics Responses

2.3.1. Equations of Motion

The concept of the augmented eigenvector of the system is introduced and defined as:

$$\mathbf{v} = \begin{bmatrix} \mathbf{v}_1 \\ \mathbf{v}_2 \end{bmatrix}; \tag{12}$$

where $\mathbf{v}_1 = [y_{1,2}, \theta_{z1,2}]^{\mathrm{T}}$, $\mathbf{v}_2 = [y_2(x)]$.

Consider a control moment $M_c(x,t)$ and a disturbance force F_d action on the beam. By using TMMMS, the equations of motion can be obtained as the following forms:

$$\mathbf{M}_1 \mathbf{v}_{1,tt} + \mathbf{C}_1 \mathbf{v}_{1,t} + \mathbf{K}_1 \mathbf{v}_1 = 0; \tag{13}$$

$$\mathbf{M}_2 \mathbf{v}_{2,tt} + \mathbf{C}_2 \mathbf{v}_{2,t} + \mathbf{K}_2 \mathbf{v}_2 = \delta_{x,L_d} F_d + \frac{\partial}{\partial x} M_c(x,t); \tag{14}$$

Table 2. First six eigenfrequencies of the system [rad/s].

Modal	1	2	3	4	5	6
TMMMS	23.50	403.85	1554.59	4033.86	7826.06	12896.02
FEM	23.50	403.85	1554.72	4036.41	7844.60	12976.42
Newton-Euler method	23.50	403.85	1554.59	4033.86	7826.06	12896.02

where

$$\begin{aligned}
\mathbf{M}_1 &= \begin{bmatrix} m & ma_{\mathrm{C}} \\ ma_{\mathrm{C}} & J_{\mathrm{I}} \end{bmatrix};\\
\mathbf{K}_1 &= \begin{bmatrix} -\mathrm{D}^3|_{\mathrm{I},1} + \mathrm{D}^3|_{\mathrm{O},1} & 0 \\ a_{\mathrm{O}}\mathrm{D}^3|_{\mathrm{O},1} & \mathrm{D}^1|_{\mathrm{I},1} - \mathrm{D}^1|_{\mathrm{O},1} \end{bmatrix};\\
\mathbf{C}_1 &= \begin{bmatrix} -\mathrm{d}^3|_{\mathrm{I},1} + \mathrm{d}^3|_{\mathrm{O},1} & 0 \\ a_{\mathrm{O}}\mathrm{d}^3|_{\mathrm{O},1} & \mathrm{d}^1|_{\mathrm{I},1} - \mathrm{d}^1|_{\mathrm{O},1} \end{bmatrix};\\
\mathbf{M}_2 &= [\bar{m}];\\
\mathbf{K}_2 &= \left[EI\frac{\partial^4}{\partial x^4}\right];\\
\mathbf{C}_2 &= [\eta];\\
\delta_{x,L_d} &= \begin{cases} 1 & x = L_d \\ 0 & \text{else} \end{cases};
\end{aligned} \tag{15}$$

$\mathbf{v}_{j,tt}$ and $\mathbf{v}_{j,t}$ are two order derivative and one order derivative of $\mathbf{v}_j$ with respect to time t, D^3, D^1, d^3, and d^1 are differential operators which are defined as following:

$$\begin{aligned}
\mathrm{D}^3|_{\alpha 1}\, y_{12} &= q_{\alpha 1};\\
\mathrm{D}^1|_{\alpha 1}\, \theta_{z1,2} &= M_{\alpha z 1};\\
\mathrm{d}^3|_{\alpha 1}\, y_{12,t} &= q^d_{\alpha 1};\\
\mathrm{d}^1|_{\alpha 1}\, \theta_{z1,2,t} &= M^d_{\alpha z 1};
\end{aligned} \tag{16}$$

$\alpha = \mathrm{I}$ denotes the input point, $\alpha = \mathrm{O}$ is the output point.

According to Eqs. (14) and (15), the equations of motion of the overall system can be written as:

$$\mathbf{M}\mathbf{v}_{tt} + \mathbf{C}\mathbf{v}_t + \mathbf{K}\mathbf{v} = \mathbf{E}_1 F_d + \mathbf{E}_2 M_c(x,t); \tag{17}$$

where

$$\begin{aligned}
\mathbf{M} &= \begin{bmatrix} \mathbf{M}_1 & \mathbf{O}_{2\times 1} \\ \mathbf{O}_{1\times 2} & \mathbf{M}_2 \end{bmatrix};\\
\mathbf{K} &= \begin{bmatrix} \mathbf{K}_1 & \mathbf{O}_{2\times 1} \\ \mathbf{O}_{1\times 2} & \mathbf{K}_2 \end{bmatrix};\\
\mathbf{E}_1 &= \begin{bmatrix} 0 & 0 & \delta_{x,L_d} \end{bmatrix}^{\mathrm{T}};\\
\mathbf{E}_2 &= \begin{bmatrix} 0 & 0 & \frac{\partial}{\partial x} \end{bmatrix}^{\mathrm{T}}.
\end{aligned} \tag{18}$$

2.3.2. Augmented Eigenvector and Eigenvector Orthogonality

The concept of the augmented eigenvector of the system is introduced and is defined as:

$$\mathbf{V}^k = \begin{bmatrix} \mathbf{V}^k_1 \\ \mathbf{V}^k_2 \end{bmatrix}; \tag{19}$$

where $\mathbf{V}^k_1 = \left[Y^k_{1,2}, \Theta^k_{z1,2}\right]^{\mathrm{T}}$. The k denotes the order of modal. Defining the inner product of $\mathbf{V}^k$ and $\mathbf{V}^p$ is:

$$\left\langle \mathbf{V}^k, \mathbf{V}^p \right\rangle = Y^k_{1,2}Y^p_{1,2} + \Theta^k_{z1,2}\Theta^p_{z1,2} + \int_0^L Y^k_2(x)\, Y^p_2(x)\, \mathrm{d}x; \tag{20}$$

The augmented eigenvector consisted of the displacement and angular displacement of joint points. The differences between augmented eigenvector and eigenvector were that the augmented eigenvector contains the displacement, angular displacement, discrete variables and continuous variables. However, the eigenvector only contained one of the displacements and the angular displacement, or contained only one of the discrete variables and the continuous variables. The numbers of variables in the augmented eigenvector equaled the number of dynamics equations of the bodies. The augmented eigenvector of the system corresponding to the eigenfrequencies $\omega_k\,(k = 1, 2, 3, \cdots)$ of the system was obtained according to the state vectors of every joint point got by solving every transfer equation of these points.

It can thus be proven that the augmented eigenvectors have the characteristics as follows:[6,7]

$$\langle \mathbf{M}\mathbf{V}^k, \mathbf{V}^p \rangle = \delta_{k,p} M_k, \quad \langle \mathbf{K}\mathbf{V}^k, \mathbf{V}^p \rangle = \delta_{k,p} K_k \ ; \tag{21}$$

where M_k represents the k-order modal mass of the system and $K_k = \omega_k^2 M_k$ denotes the modal stiffness.

2.3.3. Formulas of Dynamic Responses

Let

$$\mathbf{v} = \sum_{k=1}^{m} \mathbf{V}^k q^k(t); \tag{22}$$

where $q^k(t)$ is the generalized coordinate of the j-order modal. Due to the existence of a flexible body, the order of the system modal is $m = \infty$. We obtained a good approximation of the dynamic responses by using the cutoff modal method. By substituting Eq. (22) into Eq. (16), the dynamic response of the system can be expressed as:

$$\begin{aligned}
\sum_{k=1}^{m} \mathbf{M}\mathbf{V}^k \ddot{q}^k(t) + \sum_{k=1}^{m} \mathbf{C}\mathbf{V}^k \dot{q}^k(t) + \sum_{k=1}^{m} \mathbf{K}\mathbf{V}^k q^k(t) =\\
\mathbf{E}_1 F_d + \mathbf{E}_2 M_c(x,t).
\end{aligned} \tag{23}$$

The inner product in both sides of Eq. (21) with $\mathbf{V}^p\,(p = 1, 2, \cdots, m)$, respectively was then taken. Using the orthogonality expressed by Eq. (19), we then generalized coordinate equations of the system and obtained:

$$\begin{aligned}
\ddot{q}^k(t) + \frac{\sum_{p=1}^{m} \langle \mathbf{C}\mathbf{V}^p, \mathbf{V}^k_j \rangle}{M^k} \dot{q}^k(t) + \omega_j^2 q^k(t) =\\
\frac{\langle \mathbf{E}_1, \mathbf{V}^k \rangle F_d}{M^k} + \frac{\langle \mathbf{E}_2 M_c(x,t), \mathbf{V}^k \rangle}{M^k}.
\end{aligned} \tag{24}$$

Especially, for proportional damping, the generalized coordinate equation was written as:

$$\begin{aligned}
\ddot{q}^k(t) + 2\zeta_k\omega_k\dot{q}^k(t) + \omega_k^2 q^k(t) =\\
b^k_1 F_d(t) + F_c(t) \quad (k = 1, 2, \cdots, m);
\end{aligned} \tag{25}$$

where ζ_k represented the k-order modal damping ratio of the system, $b^k = \langle \mathbf{E}, \mathbf{V}^k \rangle / M_k$, $F_c(t) = \frac{\langle \mathbf{E}_2 M_c(x,t), \mathbf{V}^k \rangle}{M^k}$.

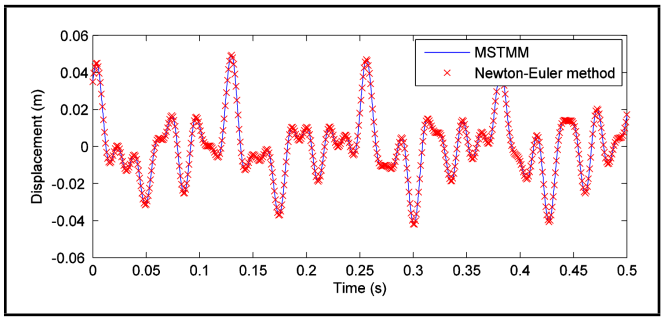

Figure 2. The computational results of the displacement of the right end of the beam.

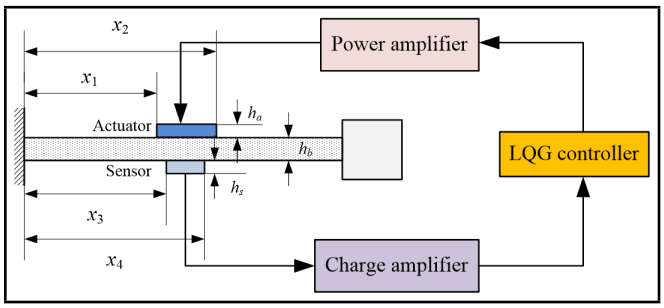

Figure 3. A sketch of the control system.

Suppose that the system suffered a force at the right end of the beam element at time instant zero while the initial displacement and velocity of the whole system was zero. The computational results obtained by the proposed method ($m = 2$) is shown in Fig. 2. In comparison, the Newton-Euler method was also implemented to solve the dynamic response. It can be seen from Fig. 2 where the computational results obtained by the above two methods are in agreement.

3. CONTROL SYSTEM DESIGN

For the purpose of designing a smart structure that responds to the environmental changes intelligently and suppresses the vibration of the system actively, an integrated control system that includes a controller, sensors, and actuators is required. However, the efficiency of the designed controller strongly depends on the position of sensors and actuators as well as their shapes and sizes. Placing the smart elements in their optimal locations can improve the controllability and observability of controller and also can reduce the required efforts to get the designed goals.[12]

In this paper, a LQG feedback controller was designed to attain the most reduction in structural responses along with the optimum controlling efforts, a piezoelectric actuator as used to supply the control force, and a piezoelectric sensor as employed to response the vibration of the system. A sketch of the control system is shown in Fig. 3.

3.1. Piezoelectric Actuator

We neglect the influence of a piezoelectric actuator and sensor on the beam due to the added lightweight material. Therefore, the induced bending moment in the piezoelectric actuator can be express in the following form:[13]

$$M_c(x,t) = \frac{1}{2}E_p d_{31}(h_a + h_b)U_c(t)\left[h(x-x_1) - h(x-x_2)\right]; \quad (26)$$

where d_{31} is referred to as the piezoelectric "strain" constant, E_p is the equivalent piezoelectric stiffness, $U_c(t)$ is the control voltage, and $h(x-x_i) = \begin{cases} 1 & x \geq x_i \\ 0 & x < x_i \end{cases}$.

By substituting Eq. (26) into Eq. (25), the generalized coordinate equation can be rewritten as:

$$\ddot{q}^k(t) + 2\zeta_k\omega_k\dot{q}^k(t) + \omega_k^2 q^k(t) = b_1^k F_d(t) + b_2^k U_c(t) \quad (k = 1, 2, \cdots, m); \quad (27)$$

where $b_2^k = \frac{1}{2}E_p d_{31}(h_a + h_b)\frac{\langle \mathbf{E}_2[h(x-x_1)-h(x-x_2)], \mathbf{V}^k\rangle}{M^k}$.

Let

$$\mathbf{x}^k = \begin{bmatrix} q^k \\ \dot{q}^k \end{bmatrix}. \quad (28)$$

By substituting Eq. (28) into Eq. (26), the state equation of the system can be given by:

$$\dot{\mathbf{x}} = \mathbf{A}\mathbf{x} + \mathrm{B}U_c + \mathbf{G}F_d; \quad (29)$$

where

$$\mathbf{x} = \begin{bmatrix} \mathbf{x}^1 \\ \vdots \\ \mathbf{x}^k \\ \vdots \\ \mathbf{x}^m \end{bmatrix}, \mathrm{B} = \begin{bmatrix} \mathrm{B}^1 \\ \vdots \\ \mathrm{B}^k \\ \vdots \\ \mathrm{B}^m \end{bmatrix}, \mathbf{G} = \begin{bmatrix} \mathbf{G}^1 \\ \vdots \\ \mathbf{G}^k \\ \vdots \\ \mathbf{G}^m \end{bmatrix}.$$

$$\mathbf{A} = \mathrm{diag}\begin{pmatrix} \mathbf{A}^1 & \cdots \mathbf{A}^k & \cdots & \mathbf{A}^m \end{pmatrix};$$

$$\mathbf{A}^k = \begin{bmatrix} 0 & 1 \\ -\omega_k^2 & -2\zeta_k\omega_k \end{bmatrix}; \mathrm{B}^k = \begin{bmatrix} 0 \\ b_2^k \end{bmatrix}; \mathbf{G}^k = \begin{bmatrix} 0 \\ {b_1}^k \end{bmatrix}.$$

3.2. Piezoelectric sensor

For a piezoelectric sensor, we have:[13]

$$D_3(x,t) = \frac{t_b E_p d_{31}}{2}\frac{\partial^2 y_2(x,t)}{\partial x^2}\left[h(x-x_3) - h(x-x_4)\right]; \quad (30)$$

where D_3 is the electric displacement of the piezoelectric sensor. Therefore, the output of the sensor can be given by:

$$y(t) = \int_0^L wD_3(x,t)\,\mathrm{d}x = \frac{t_b E_p d_{31} w}{2}\int_0^L \frac{\partial^2 y_2(x,t)}{\partial x^2}\left[h(x-x_3) - h(x-x_4)\right]\mathrm{d}x; \quad (31)$$

where w is the width of the sensor.

Eq. (31) can be rewritten as:

$$y(t) = \frac{t_b E_p d_{31} w}{2}\langle \mathbf{a}, \mathbf{v}\rangle; \quad (32)$$

where $\mathbf{a} = \begin{bmatrix} 0 & 0 & \frac{\partial^2}{\partial x^2} \end{bmatrix}^{\mathrm{T}}$.

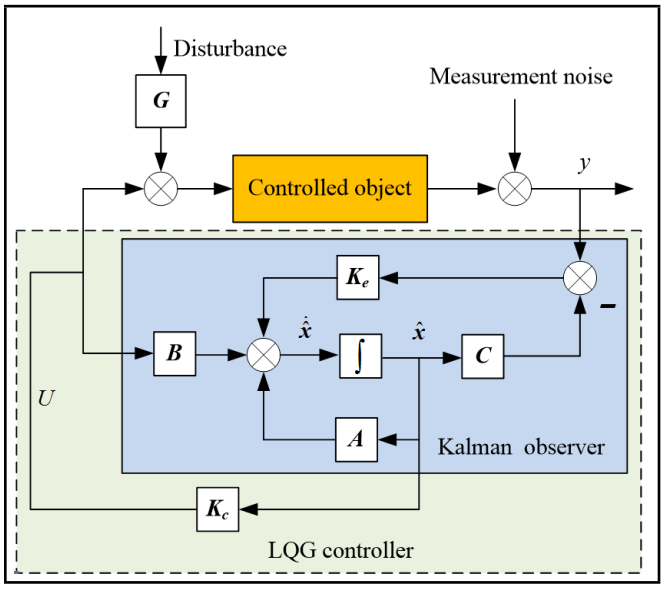

Figure 4. Structure of the LQG controller.

By substituting Eq. (22) to Eq. (32), the system output can be expressed by:

$$y = \frac{t_b E_p d_{31} w}{2} \sum_{k=1}^{m} \langle \mathbf{a}, \mathbf{V^k} \rangle \mathbf{q^k(t)}. \tag{33}$$

Equation (33) can be rewritten as:

$$y = \mathbf{Cx}; \tag{34}$$

where $\mathbf{C} = \begin{bmatrix} \mathbf{c}^1 & \mathbf{c}^2 & \cdots & \mathbf{c}^m \end{bmatrix}$, $\mathbf{c}^k = \begin{bmatrix} c^k & 0 \end{bmatrix}$, $c^k = \frac{t_b E_p d_{31} w}{2} \langle \mathbf{a}, \mathbf{V}^k \rangle$. Therefore, the control equation can be expressed by:

$$\begin{cases} \dot{\mathbf{x}} = \mathbf{Ax} + \mathrm{B}U_c + \mathbf{G}F_d \\ y = \mathbf{Cx} \end{cases}. \tag{35}$$

3.3. LQG Controller

The LQG controller, which is shown in Fig. 4, is a combination of the linear quadratic regulator and the Kalman filter. The controller design using the linear quadratic regulator is discussed in this section. Due to various uncertainties, the system dynamics is not constant. The LQG control is an excellent robust control system design methodology. Let the system to be controlled be written in state-space form given below:

$$\begin{matrix} \dot{\mathbf{x}} = \mathbf{Ax} + \mathrm{B}U_c + \mathbf{G}F_d \\ y = \mathbf{Cx} + \eta \end{matrix}; \tag{36}$$

where η is the measurement noise and process noise, both F_d and η are the zero mean Gaussian white noise and is mutually unrelated.

The linear quadratic optimal control problem is to find the input $U_c(t)$ to the plant such that a scalar quadratic cost function:

$$J = \mathrm{E}\left[\int_0^\infty \left(\mathbf{x}^{\mathrm{T}} \mathbf{Q} \mathbf{x} + RU^2 \right) \mathrm{d}t \right]; \tag{37}$$

where $\mathbf{Q}$ is a symmetric positive semi-definite matrix, and R is a positive constant.

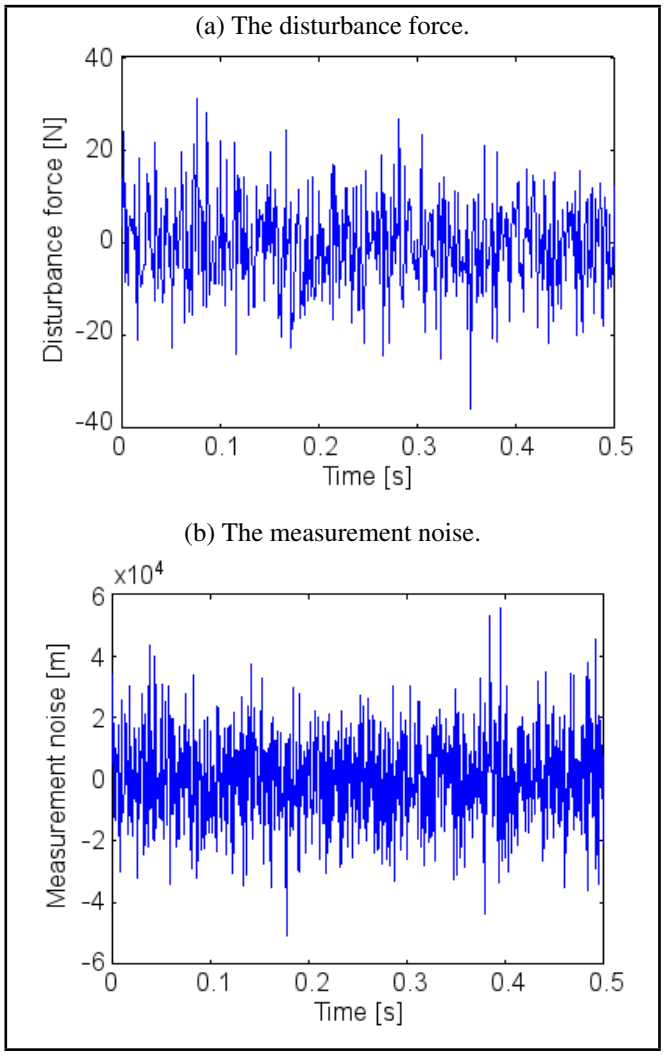

Figure 5. The disturbance force and measurement noise.

The structure of the LQG controller is shown in Fig. 4. The Kalman state observer can be expressed by:

$$\dot{\hat{\mathbf{x}}} = \mathbf{A}\hat{\mathbf{x}} + \mathbf{B}U_c + \mathbf{K}_{\mathrm{e}} \left(y - \mathbf{C}\hat{\mathbf{x}} \right); \tag{38}$$

where $\mathbf{K}_{\mathrm{e}}$ is the gain matrix of the state observer.

The state equation of the control system can be given by:

$$\begin{matrix} \dot{\hat{\mathbf{x}}} = \left(\mathbf{A} - \mathbf{B}\mathbf{K}_c - \mathbf{K}_{\mathrm{e}}\mathbf{C} \right) \hat{\mathbf{x}} + \mathbf{K}_{\mathrm{e}} y \\ U_c = -\mathbf{K}_{\mathrm{c}} \hat{\mathbf{x}} \end{matrix}; \tag{39}$$

where $\mathbf{K}_{\mathrm{e}}$ and $\mathbf{K}_c$ can be satisfied the Riccati equations:

$$\mathbf{AS}_{\mathrm{e}} + \mathbf{S}_{\mathrm{e}}\mathbf{A}^{\mathrm{T}} - \frac{1}{R_1}\mathbf{S}_{\mathrm{e}}\mathbf{C}^{\mathrm{T}}\mathbf{C}\mathbf{S}_e + \mathbf{Q}_1 = \mathbf{O}$$

$$\text{and} \quad \mathbf{K}_{\mathrm{e}} = \frac{1}{\mathrm{R}_1}\mathbf{S}_{\mathrm{e}}\mathbf{C}^{\mathrm{T}}; \tag{40}$$

$$\mathbf{S}_{\mathrm{c}}\mathbf{A} + \mathbf{A}^{\mathrm{T}}\mathbf{S}_{\mathrm{c}} - \frac{1}{R_2}\mathbf{S}_{\mathrm{c}}\mathbf{B}\mathbf{B}^{\mathrm{T}}\mathbf{S}_{\mathrm{c}} + \mathbf{Q}_2 = \mathbf{O}$$

$$\text{and} \quad \mathbf{K}_{\mathrm{c}} = \frac{1}{\mathrm{R}_2}\mathbf{B}^{\mathrm{T}}\mathbf{S}_{\mathrm{c}}. \tag{41}$$

Apply a disturbance force, as seen in Fig. 5a, to the system. The measurement noise, which is shown in Fig. 5b, has been considered as with zero mean. The estimated value $\hat{\mathbf{x}}$ and the actual value $\mathbf{x}$ are plotted in Fig. 6, which indicates the Kalman observer can effectively estimate the state vector.

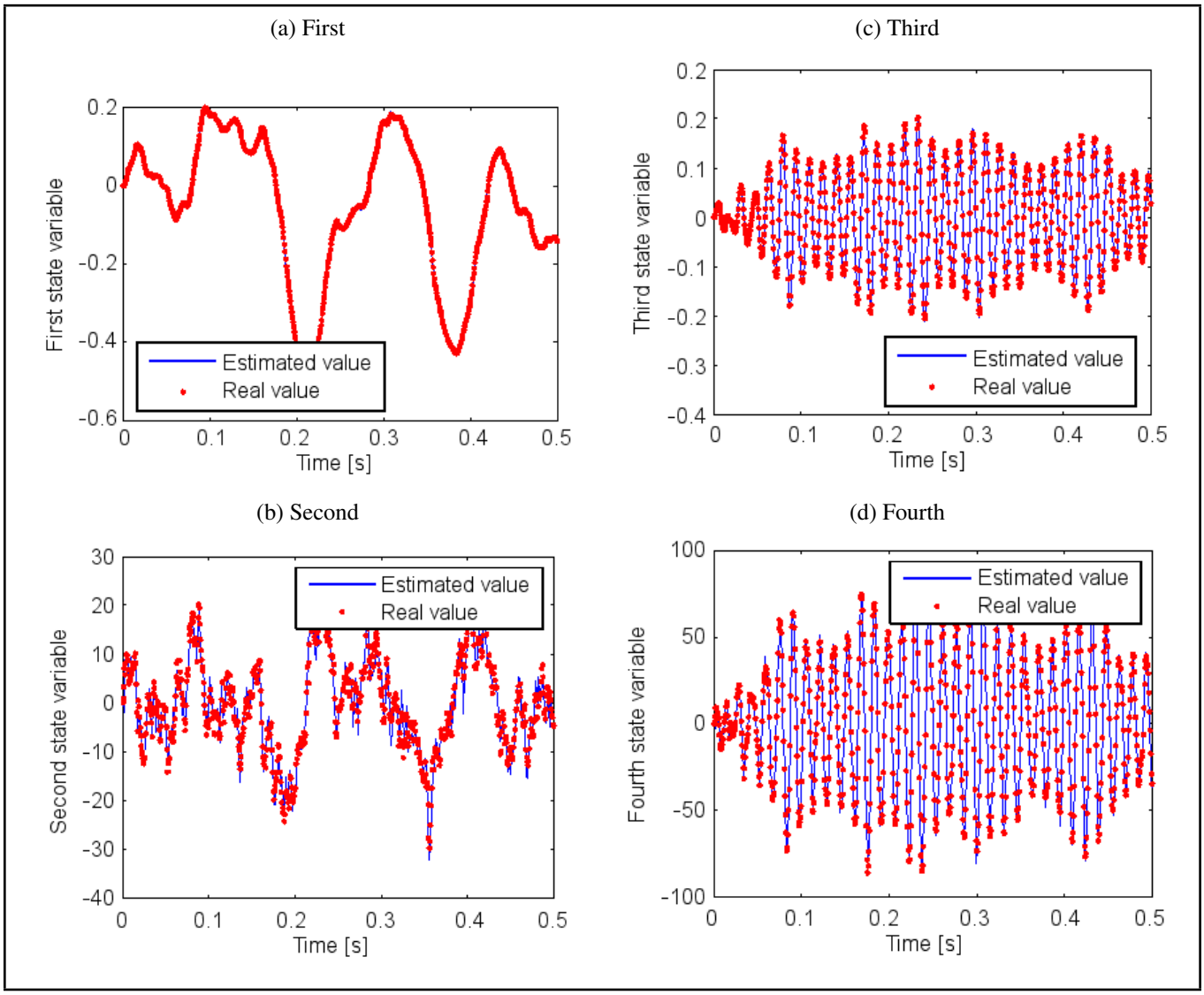

Figure 6. Results of the Kalman observer.

4. EXPERIMENTAL VERIFICATION

4.1. Experimental Setup

In order to experimentally validate the proposed LQG controller, the experimental setup is shown in Fig. 7. It can be seen from Fig. 7 that the experimental setup is composed of the controlled object (the cantilever beam with an eccentric tip mass), piezoelectric sensor, actuator (PZT-5H), charge amplifier (type 5018, Kistler corporation), piezoelectric power amplifier (type XE-503, Harbin Core Tomorrow corporation), vibration exciter (type: JZK-50, maximum output force: 500 N, power amplifier: YE5874A, Sinocera corporation), Function generator (type: 33220A, Agilent corporation), real-time simulation system (dSPACE DS1006 with MATLAB/Simulink), 16 bit A/D (type: DS2004), 16 bit D/A (type: DS2103), and laser Doppler vibrometer (LDV, type: PVS-505/OFV-5000, Polytec corporation). When conducting experiments, the controlled object, that has an output that is monitored by the piezoelectric sensor and sent to the charge amplifier, is driven by the piezoelectric power amplifier. The voltage applied to the power amplifier and the output from the charge amplifier are acquired to the host computer by the real-time simulation system. The disturbance force is generated by the vibration exciter. The LDV is

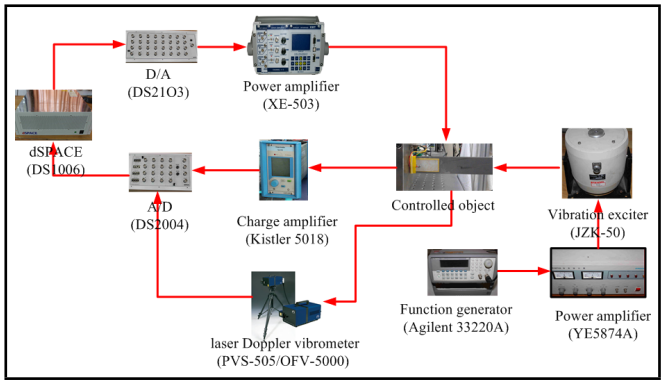

Figure 7. The experimental setup.

used to measure the output displacement of the P point shown in Fig. 1 to validate the piezoelectric sensor.

4.2. Experimental results

4.2.1. System Parameters

The parameters of the piezoelectric sensor and actuator are listed in Tab. 4.2.1. Other parameters of the controlled object are given in Tab. 2.2. The parameters of the controller are listed in Tab. 4.

Table 3. Parameters of the piezoelectric sensor and actuator (PZT-5H).

$d_{31} = -320 \times 10^{-12}\,\mathrm{m/V}$	$E_p = 6.2 \times 10^{10}\mathrm{Pa}$	$x_1 = 0.1\mathrm{m}$
$x_2 = 0.155\mathrm{m}$	$x_3 = 0.12\mathrm{m}$	$x_4 = 0.13\mathrm{m}$
$h_a = 0.005\mathrm{m}$	$h_s = 0.005\mathrm{m}$	$h_b = 0.05\mathrm{m}$
$w = 0.005\mathrm{m}$	$L_d = 0.04\mathrm{m}$	

Table 4. Parameters of the LQG controller.

$\mathbf{K_e} = [3.3 \times 10^7 \quad 1.9 \times 10^{11} \quad 4.2 \times 10^7 \quad 2.4 \times 10^{11}]^{\mathrm{T}}$
$\mathbf{K_c} = [3.7102 \quad 0.1087 \quad 0.1969 \quad 0.0034]$

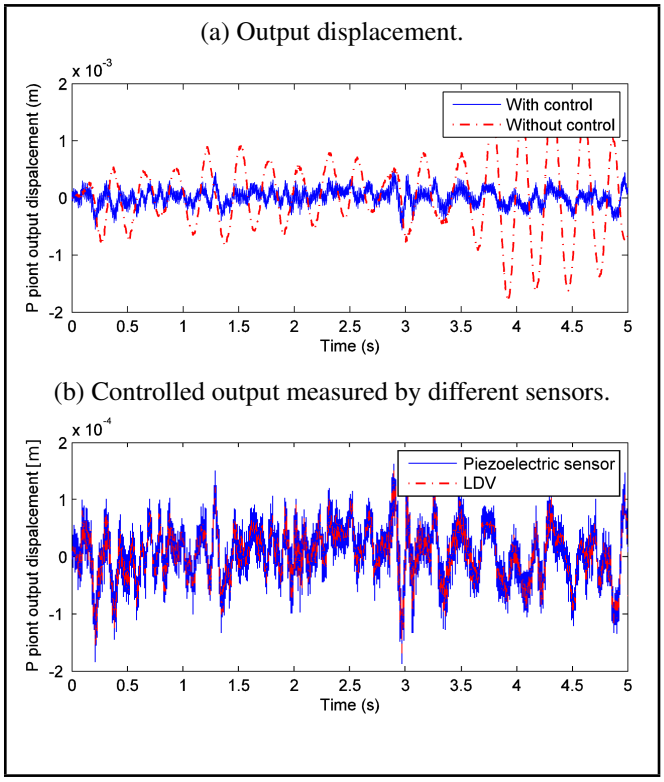

Figure 8. Controlled and uncontrolled output displacements of the P-point under a zero mean Gaussian white noise excitation.

4.2.2. Control results and analysis

Under a zero mean Gaussian white noise excitation, an impulse excitation, and a 100 Hz sinusoidal excitation, the controlled and uncontrolled results are shown in Figs. 8 to 10, respectively, which indicate that the LGQ controller can effectively control the vibration responses of the controlled system under an arbitrary excitation and the piezoelectric sensor can measure vibration responses with high-accuracy.

It can be seen from Figs. 8 to 10, the maximum output displacement with the control are reduced to 83.3% and 62.5% relative to without control under the white noise excitation and the sinusoidal excitation, respectively. The reason is that when designing the LGQ controller, we considered the disturbance force to have a zero mean Gaussian white noise excitation.

According to Figs. 8 to 10, the quantitative measurement errors under different excitations are listed in Tab. 5. From Tab. 5, the maximum relative error is 1.22%, which may result from the nonlinearity of the piezoelectric sensor and the modeling error.

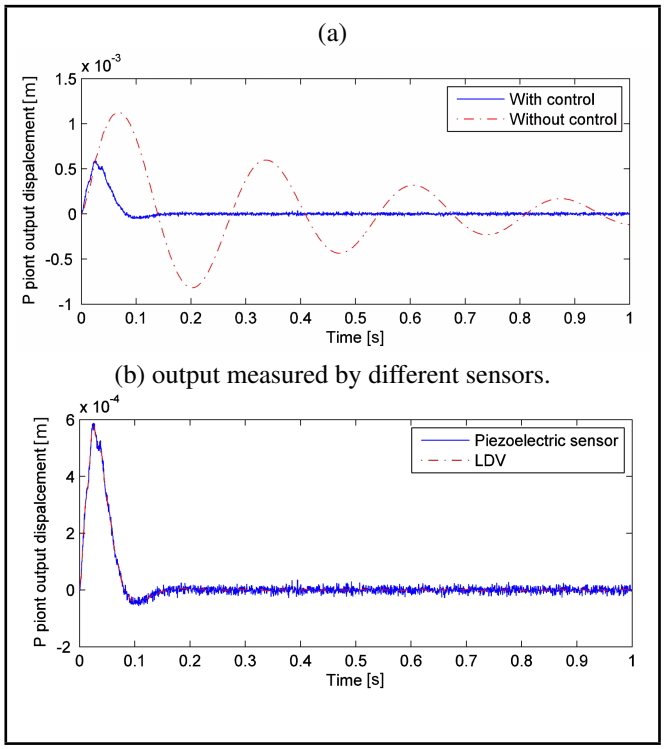

Figure 9. Controlled and uncontrolled output displacements of the P-point under an impulse excitation.

Table 5. Quantitative measurement errors.

Excitation	Measurement error
white noise	1.22%
impulse	1.01%
sinusoidal	1.02%

5. CONCLUSIONS

In order to control of the vibration responses of a cantilever beam carrying a concentrated mass, a novel model was first put forward to describe dynamics characteristics of using the transfer matrix TMMMS. Based on this proposed model, a LQG controller for that system was then established and theoretically analyzed. Finally, the experimental results showed that the proposed controller can effectively reduce the vibration of the cantilever beam with an eccentric tip mass. Therefore, this new model gave a broad range of possibilities for model-based controller design and implementation.

Future work can be performed in the direction of using the proposed method in some mechanical systems. For instance, wind tunnel stings carrying an airplane. Considering using and optimizing multiple actuators and sensors may also be a good idea.

ACKNOWLEDGEMENTS

The authors wish to acknowledge the financial support by National Natural Science Foundation of China (Grant No.61304137), the Fundamental Research Funds for the Central Universities (Grant No. 30915011326), the Scientific Research Foundation of Nanjing University of Posts and Telecommunications (Grant No. NY213111), the Key University Science Research Project of Jiangsu Province (Grant No. 15KJB130005), and the Basic Scientific Research of National Defense (JCKY201606C001).

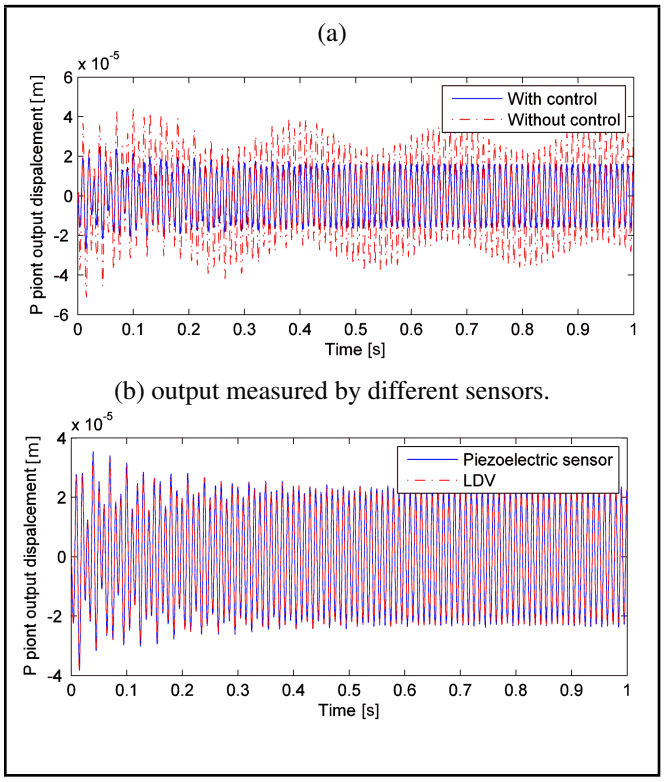

Figure 10. Controlled and uncontrolled output displacements of the P-point under a 100 Hz sinusoidal excitation.

REFERENCES

[1] Yaman M. A domain decomposition method for solving a cantilever beam of varying orientation with tip mass, *J. Comput. Nonlinear Dyn.*, **2** (1), 52–58, (2007).

[2] To C. W. S. Vibration of a cantilever beam with a base excitation and tip mass, *J. Sound Vib.*, **83** (4), 445–460, (1982).

[3] Rama Bhat B., Wagner, H. Natural frequencies of a uniform cantilever with a tip mass slender in the axial direction, *J. Sound Vib.*, **45** (2), 304–307, (1976).

[4] Matt, C. F. On the application of generalized integral transform technique to wind-induced vibrations on overhead conductors, *Int. J. Numer. Methods Eng.*, 78 (8), 901–930, (2009).

[5] Song, G., Zhao, J. Q., Zhou, X. Q., and Alexis De Abreu-Garca J. Tracking control of a piezoceramic actuator with hysteresis compensation using inverse Preisach model, *IEEE/ASME Transactions on Mechatronics*, **10** (2), 198–209, (2005).

[6] Matt, C. F. T. Simulation of the transverse vibrations of a cantilever beam with an eccentric tip mass in the axial direction using integral transforms, *Applied Mathematical Modelling*, **37**, 9338–9354, (2013).

[7] Singhose, W. Command shaping for flexible systems: A review of the first 50 years, *International Journal of Precision Engineering and Manufacturing*, **10** (4), 153–168, (2009)

[8] Song, G., Schmidt, S. P., and Agrawal, B. N. Experimental robustness study of positive position feedback control for active vibration suppression, *J. Guid. Control Dyn.*, **25**, 179–82, (2002).

[9] Meyer, J. L., Harrington, W. B., Agrawal, B. N., and Song, G. Vibration suppression of a spacecraft flexible appendage using smart material, *Smart Mater. Struct.*, **7**, 95–104, (1998).

[10] Shan, J. J., Liu, H. T., and Sun, D. Slewing and vibration control of a single-link flexible manipulator by positive position feedback (PPF), *Mechatronics*, **15**, 487–503, (2005).

[11] Rossit, C. A. and Laura, P. A. A. Free vibrations of a cantilever beam with a spring-mass system attached to the free end, *Ocean Eng.*, **28** (7), 933–9, (2001).

[12] Fason, J. L. and Cuaghey, T. K. Positive position feedback for control of larges space structures, *AIAA Journal*, **28** (4), 717–724, (1990).

[13] Song, G., Schmidt, S. P., and Agrawal, B. N. Experimental robustness study of positive position feedback control for active vibration suppression, *Journal of Guidance, Control, and Dynamics*, **25** (1), 179–182, (2002).

[14] Fanson, J. L. *An experimental investigation of vibration suppression in large space structures using positive position feedback*, PhD Thesis, California Inst. of Technology, Pasadena, CA, (1986).

[15] Meyer, J. L., Harrington, W. B., Agrawal, B. N., and Song, G. Vibration suppression of a spacecraft flexible appendage using smart material, *Smart Materials and Structures*, **7** (1), 95–104, (1998).

[16] Shan, J. J., Liu, H. T., and Sun, D. Slewing and vibration control of a single-link flexible manipulator by positive position feedback (PPF), *Mechatronics*, **15** (4), 487–503, (2005).

[17] Preumont, A. *Vibration control of active structures: An introduction,* Kluwer Academic, Norwell, MA, 101–103, (2007).

[18] Singhose, W., Eloundou, R., and Lawrence, J. Command generation for flexible systems by input shaping and command smoothing, *Journal of Guidance, Control, and Dynamics*, **33** (6), 1697–1707, (2010).

[19] Rui, X. T., Wang, G. P., Lu, Y. Q., Yun, L. F., Transfer matrix method for linear multibody system, *Multibody Syst. Dyn.*, **19** (3), 179–207, (2008).

[20] Rui, X. T., Zhang, J. S., and Zhou, Q. B. Automatic deduction theorem of overall transfer equation of multibody system, *Advances in Mechanical Engineering*, **6**, 1–12, (2014). http://dx.doi.org/10.1155/2014/378047

[21] Preumont A. *Vibration control of active structures-an introduction*, Second ed., Kluwer Academic Publishers, (2002).